JACS
JOURNAL OF THE AMERICAN CHEMICAL SOCIETY
Article
pubs.acs.org/JACS

Competition between Singlet Fission and Charge Separation in Solution-Processed Blend Films of 6,13-Bis(triisopropylsilylethynyl)-pentacene with Sterically-Encumbered Perylene-3,4:9,10-bis(dicarboximide)s

Charusheela Ramanan,[†] Amanda L. Smeigh,[†] John E. Anthony,[‡] Tobin J. Marks,*[,†] and Michael R. Wasielewski*[,†]

[†]Department of Chemistry and Argonne−Northwestern Solar Energy Research (ANSER) Center, Northwestern University, Evanston, Illinois 60208-3113, United States

[‡]Department of Chemistry, University of Kentucky, Lexington, Kentucky 40506-0055, United States

Supporting Information

ABSTRACT: The photophysics and morphology of thin films of *N*,*N*-bis(2,6-diisopropylphenyl)perylene-3,4:9,10-bis(dicarboximide) (**1**) and the 1,7-diphenyl (**2**) and 1,7-bis(3,5-di-*tert*-butylphenyl) (**3**) derivatives blended with 6,13-bis(triisopropylsilylethynyl)pentacene (TIPS-Pn) were studied for their potential use as photoactive layers in organic photovoltaic (OPV) devices. Increasing the steric bulk of the 1,7-substituents of the perylene-3,4:9,10-bis(dicarboximide) (PDI) impedes aggregation in the solid state. Film characterization data using both atomic force microscopy and X-ray diffraction showed that decreasing the PDI aggregation by increasing the steric bulk in the order **1** < **2** < **3** correlates with a decrease in the density/size of crystalline TIPS-Pn domains. Transient absorption spectroscopy was performed on ∼100 nm solution-processed TIPS-Pn:PDI blend films to characterize the charge separation dynamics. These results showed that selective excitation of the TIPS-Pn results in competition between ultrafast singlet fission (^{1}*TIPS-Pn + TIPS-Pn → 2 ^{3}*TIPS-Pn) and charge transfer from ^{1}*TIPS-Pn to PDIs **1**−**3**. As the blend films become more homogeneous across the series TIPS-Pn:PDI **1** → **2** → **3**, charge separation becomes competitive with singlet fission. Ultrafast charge separation forms the geminate radical ion pair state ^{1}(TIPS-Pn$^{+\bullet}$−PDI$^{-\bullet}$) that undergoes radical pair intersystem crossing to form ^{3}(TIPS-Pn$^{+\bullet}$−PDI$^{-\bullet}$), which then undergoes charge recombination to yield either ^{3}*PDI or ^{3}*TIPS-Pn. Energy transfer from ^{3}*PDI to TIPS-Pn also yields ^{3}*TIPS-Pn. These results show that multiple pathways produce the ^{3}*TIPS-Pn state, so that OPV design strategies based on this system must utilize this triplet state for charge separation.

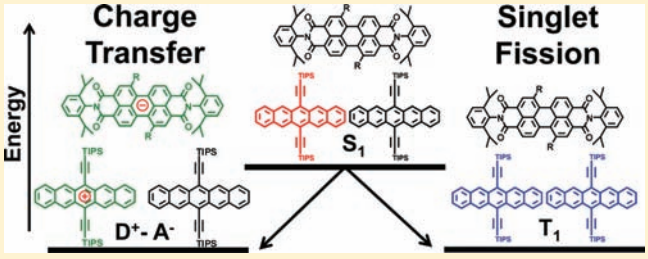

INTRODUCTION

The photoactive layers in organic photovoltaic (OPV) cells comprise electron-donor (D) and electron-acceptor (A) molecules with relative molecular orbital energies suitable for exciton creation, subsequent exciton dissociation at the D−A interface, and then diffusion-controlled charge collection at the OPV electrodes.[1] In many current-generation OPVs, these layers include a semiconducting polymer donor, such as poly(3-hexyl)thiophene (P3HT) or the more recently reported poly(thieno[3,4-*b*]thiophene-*alt*-benzodithiophene) (PTB) class, and a fullerene acceptor, such as [6,6]-phenyl-C_{61}-butyric acid methyl ester (PCBM). In optimized devices, these D−A combinations provide power conversion efficiencies (PCEs) of ∼5% and ∼7%, respectively.[2] These OPV photoactive materials are typically solution-processed from mixed D−A solutions to create bulk heterojunction (BHJ) active layers having interpenetrating electron-donor (hole-transporting) and electron-acceptor (electron-transporting) networks. Such composites result in far larger D−A contact areas than in simple D−A bilayers, yielding OPVs that exhibit greater exciton dissociation and charge separation efficiencies and hence greatly increased device PCEs.[1a,3] Materials-oriented research to create OPVs having larger PCEs is currently focused on the transparent conductive oxide anode,[4] the interfaces between the device layers,[5] and the materials within the photoactive layer.[6] While many new semiconducting polymer[7] and small-molecule[8] donors have been developed, there has been a paucity of effective new acceptors. The relatively high performance of OPVs having fullerene acceptors is attributed in part to the molecular geometries, which promote efficient mixing with the donor polymer to form optimal molecular interfaces for exciton separation and subsequent charge transport.[9] However, fullerene derivatives also have undesirable properties, including

Received: August 25, 2011
Published: November 23, 2011

   dx.doi.org/10.1021/ja2080482 | *J. Am. Chem.Soc.* 2012, 134, 386−397

relatively low extinction coefficients for light absorption at visible and near-IR wavelengths[6a,10] as well as the tendency to degrade in the presence of air and moisture.[11]

Perylene-3,4:9,10-bis(dicarboximide)s (PDIs) (Figure 1a) offer a number of attractive characteristics as OPV electron

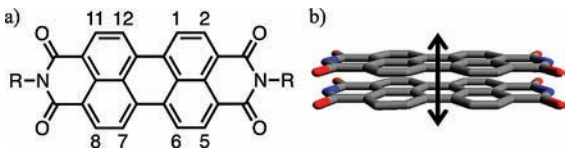

Figure 1. (a) Chemical structure of PDIs and (b) illustration of cofacial π-stacking of two PDI molecules.

acceptors, including favorable orbital energetics, high extinction coefficients in the visible spectral region,[12] photostability,[13] and the capacity to self-assemble into ordered nanostructures.[14] PDIs have previously been used as solution-processable, high mobility, air-stable n-type semiconductors and are readily modified using straightforward synthetic routes.[15] Furthermore, previous reports have demonstrated charge separation in PDI acceptors blended with thiophene[16] and fluorene[17] polymer donors. Other work has paired PDI with a liquid-crystalline hexabenzocoronene derivative,[18] where transient microwave photoconductivity studies showed that exciton−exciton annihilation competes with charge separation, limiting the device efficiency.[19] This is consistent with the fact that OPV studies incorporating PDI acceptors have generally been limited in comparison with studies of fullerene acceptors.[1b,6c,20] The relatively poor device performance of PDI derivatives observed to date in solution-processed devices is attributed to the well-known propensity of these molecules to form π-stacked aggregates (Figure 1b).[13,21] While the tendency of the PDIs to aggregate via π-stacking interactions is advantageous in increasing the electron mobility,[22] these aggregates may diminish OPV performance by creating unfavorable nanostructures that quench excitons within the photoactive layer.[17] Such effects are particularly pronounced in solution-processed devices, where PDI aggregates can precipitate from solution in a broad distribution of aggregate sizes. A recent study of the photophysical and OPV characteristics of PDI-containing devices fabricated with three different donor polymers showed that the PDI acceptor is aggregated to varying degrees.[17b] It was found that disrupting the PDI π-stacking actually affords morphologies more favorable for charge extraction and that the device efficiency is limited by fast bimolecular recombination or by enhanced PDI exciton relaxation due to the formation of excimer-like states in PDI *H*-aggregates.[17a] These results are consistent with our earlier studies on discrete cofacial π-stacked PDI oligomers, which showed that excimer-like states form at a rate that is dependent on the degree to which two or more PDIs can tightly π-stack in an *H*-aggregate geometry.[23]

Recent work has highlighted the importance of electronic and molecular interactions at the OPV D−A interface.[24] Perez et al.[25] showed that changes in the molecular structure at the D−A interface in bilayer small-molecule OPVs result in large variations in device open-circuit voltage (V_{oc}) and the dark current, and Erwin and Thompson[26] recently corroborated these results with a series of PDI acceptors. Kim et al.[27] showed that decreasing the PDI π-stacking correlates with decreased interfacial radial ion pair recombination in bilayer-architecture OPV devices. This same work also highlighted the importance of not diminishing PDI−PDI molecular interactions too greatly, since this suppresses the charge separation efficiency.

Earlier work reported promising OPV performance when a PDI acceptor was paired with a pentacene (Pn) donor in vapor-deposited bilayer structures.[28] Pn-based devices have received significant attention recently because Pn is known to undergo singlet fission (SF).[29] This is a process by which a singlet exciton is converted into two independent triplet excitons, with the result that if both triplet excitons inject charge into a semiconductor electrode quantitatively, the maximum theoretical thermodynamic efficiency of a single-junction solar cell (the Queisser−Shockley limit) rises from 32% to 46%.[30] Singlet fission was first proposed in 1965 to explain delayed fluorescence in anthracene crystals[31], then invoked in crystalline tetracene to rationalize its low fluorescence quantum yield, and subsequently confirmed in pentacene crystals.[32] Singlet fission has been observed in mixed crystals (hetero-fission) of anthracene doped with tetracene[33] and pentacene doped with tetracene.[32b] More recently, crystalline *p*-terphenyl, *p*-sexiphenyl,[34] tetracyano-*p*-quinodimethane,[17,18] 1,3-diphenyl-isobenzofuran,[35] perylene,[36] benzophenone,[37] and rubrene[38] have all been shown to undergo singlet fission with triplet quantum yields (Φ_T) ranging from 6 to 200%. Singlet fission has also been observed in carotenoid aggregates with high efficiency[39] and in selected aromatic polymers.[24,25,40] While significant computational work has been done to predict the optimal molecular structures for SF,[41] only one designer SF chromophore has been studied experimentally.[35] In addition, there has also been only one report on charge separation in a pentacene/fullerene bilayer resulting from triplet excitons produced by SF.[29b] While there have been a few recent reports exploring SF in OPVs,[29b,42] SF chromophores have not been widely used in these devices because a fundamental understanding of the factors that control the SF efficiency in molecular solids is lacking.

The SF rate is maximized when the sum of the energies of the two triplet excitons (T_1) is lower than that of the vibrationally relaxed singlet state (S_1) [i.e., when $E(S_1) > 2E(T_1)$]. Once SF produces two triplet excitons, T_1-T_1 annihilation can be a serious problem if the triplet excitons cannot diffuse apart quickly. However, when $E(S_1) > 2E(T_1)$, the rate of T_1-T_1 annihilation to yield S_1 and S_0 is slow because this process is endergonic. In addition to these energetic requirements, it is clear that intermolecular electronic coupling and orientation are also critical for efficient SF, but only two series of systematic studies varying these conditions have been reported.[35,41b,43] Theoretical work has suggested that a cofacial, $\pi-\pi$ slip-stacked relationship between chromophores facilitates high SF efficiency.[29c]

To explore the effects of PDI π-stacking modulation on charge separation and recombination processes in solution-processed thin films, PDI derivatives **1**−**3** (Figure 2) with variable steric encumbrance to π-stacking were synthesized, characterized, and studied as blends with the soluble donor 6,13-bis(triisopropylsilylethynyl)pentacene (TIPS-Pn) (Figure 2).[44] This solubilized polyacene has been used previously in organic field-effect transistors.[45] However, its use in OPVs has had modest success, and bilayer-type devices using a fullerene acceptor exhibit PCEs of ~0.5%.[46] Comparison with other functionalized Pn derivatives has demonstrated a very slight improvement in device parameters with impeded pentacene crystallinity.[46a] In addition, the performance of TIPS-Pn in BHJ devices is limited because of its tendency to form Diels−Alder

dx.doi.org/10.1021/ja2080482 | J. Am. Chem.Soc. 2012, 134, 386−397

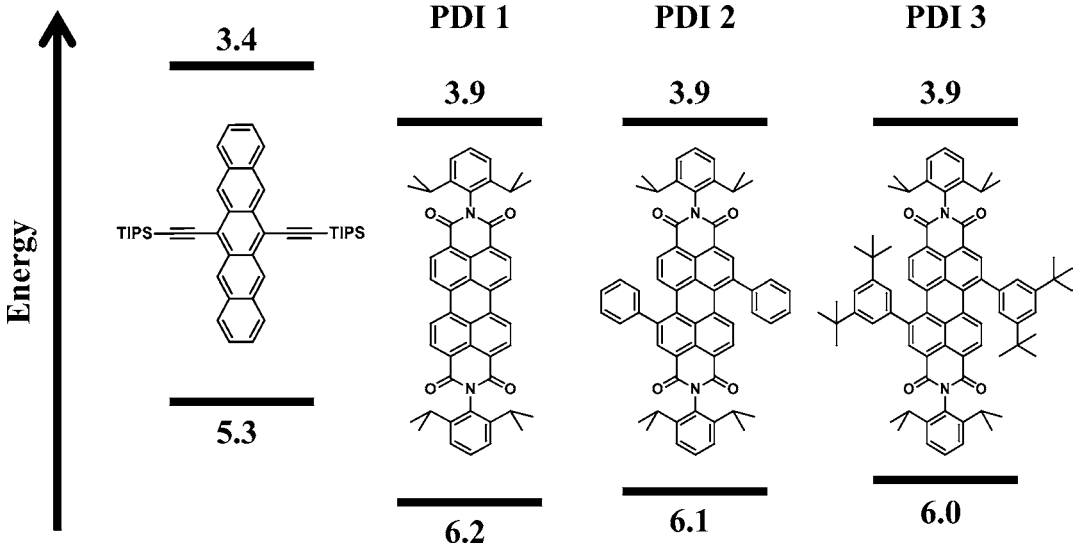

Figure 2. Molecular structures and HOMO/LUMO energies, as determined by electrochemistry and optical band gap measurements, of the PDI electron acceptors **1**–**3** and the TIPS-Pn electron donor.

adducts with solubilized fullerenes in solution.[47] This undesirable chemistry does not occur with the PDI acceptors examined here.

The blend films as well as neat films of each component material were characterized here by transient absorption spectroscopy over the femtosecond-to-microsecond time range. The charge separation and recombination dynamics are correlated with the film morphology, as determined by atomic force microscopy (AFM) and X-ray diffraction (XRD) measurements. The film characterization and steady-state optical absorption and fluorescence measurements confirmed the variable tendency to undergo π-stacking across the series PDI **1** → **2** → **3**. Transient absorption spectroscopy of TIPS-Pn in solution and films was also investigated, revealing that neat TIPS-Pn films undergo ultrafast singlet fission. Furthermore, sterically encumbered PDIs **2** and **3** provide improved film morphologies and enhanced D–A electronic interactions, suppressing SF and promoting more efficient charge separation. Thus, the present synthetic modifications of PDI electron acceptors can be used to address those mechanisms that limit the performance of OPVs incorporating them.

EXPERIMENTAL SECTION

Synthesis. The synthesis and characterization of PDI derivatives **1**–**3** are described in the Supporting Information. All of the final PDI products were purified by gradient sublimation at 350 °C/10^{-6} Torr. TIPS-Pn was purified by recrystallization (2×) from acetone.

Cyclic Voltammetry and Spectroelectrochemistry. Cyclic voltammetry was carried out using a CH Instruments model 622 electrochemical workstation. All measurements were performed in dry dichloromethane containing 0.1 M tetra-*n*-butylammonium hexafluorophosphate ($TBAPF_6$) as the supporting electrolyte. The solutions were purged with N_2 to ensure an O_2-free environment. Measurements were obtained using a 1.0 mm diameter platinum disk working electrode, a platinum wire counter electrode, and a silver wire reference electrode. Spectroelectrochemistry was performed using a platinum mesh working electrode, a platinum wire counter electrode, and a silver wire reference electrode in a 2 mm path length cuvette. For all electrochemical measurements, the ferrocene/ferrocenium (Fc/Fc^+) redox couple (0.46 V vs SCE in CH_2Cl_2[48]) was used as an internal reference.

Film Fabrication and Characterization. Glass slides were first cleaned with detergent, water, and acetone in sequence and then subjected to UV/O_3 treatment to improve film wetting by the organic solvent. Equimolar 20 mg/mL solutions of TIPS-Pn and each PDI were mixed in toluene and spin-cast onto 0.5 mm thick glass cover slides to give ~100 nm thick organic films. Films of neat TIPS-Pn and PDIs **1**–**3** (80–90 nm thick) were also fabricated using the same procedure. The films were characterized by AFM using a Veeco Dimension ICON PT system, XRD using a Rigaku ATX-G thin-film diffraction workstation, and profilometry using a Veeco Dektak 150 surface profiler.

Photophysical Measurements. Steady-state UV–vis spectra were obtained with a Shimadzu 1800 spectrophotometer and fluorescence measurements with a PT1 Quanta-Master 1 single-photon spectrofluorimeter in a right-angle configuration. Femtosecond transient absorption (fsTA) measurements were made using a 2 kHz Ti-sapphire laser system as detailed previously.[49] The instrument response function for the pump–probe experiments was 150 fs. The transient spectra were obtained using 5 s of averaging at a given delay time, and the pump intensity was maintained at 0.5 μJ/pulse (200 μm diameter spot size at the sample). The nanosecond transient absorption (nsTA) apparatus has been described previously;[14a] however, the excitation laser used was a Spectra-Physics Lab-150 laser coupled to a Basi-scan optical parametric oscillator (OPO) (Spectra-Physics). The OPO output was directed onto the sample and focused to a beam (1.5 mJ/pulse; 1 cm diameter spot size at the sample) slightly larger than the probe beam, ensuring efficient pump–probe overlap. Fifty transients were averaged at 5 nm intervals spanning 400–800 nm. The transient spectra were constructed by plotting specific time points of each kinetic trace with respect to the corresponding wavelength. Solution nsTA experiments were performed in toluene, and samples were degassed by five freeze–pump–thaw cycles. For both fsTA and nsTA, the photoinduced processes were studied using both 532 and 650 nm excitation wavelengths. Analysis of kinetic data was performed at multiple wavelengths using a Levenberg–Marquardt nonlinear least-squares fit to a general sum-of-exponentials function with a Gaussian convolution to account for the finite instrument response.

RESULTS AND DISCUSSION

Energetics of Charge Separation. The redox potentials of TIPS-Pn and PDIs **1**–**3** were measured by cyclic voltammetry and are summarized in Table 1. These measurements were used in conjunction with the optical band gap (E_g) to characterize the HOMO/LUMO energies of the materials,[50] and these results are shown in Figure 2. The results

dx.doi.org/10.1021/ja2080482 | J. Am. Chem.Soc. 2012, 134, 386–397

Table 1. Redox and Excited-State Data for the TIPS-Pn Donor and the PDI Acceptors 1−3

	E_{ox} (eV)[a]	E_{red1} (eV)[a]	E_{red2} (eV)[a]	λ_{abs} (nm)	λ_{em} (nm)	E_g (eV)[b]	E_{HOMO} (eV)[c]	E_{LUMO} (eV)[c]
TIPS-Pn	0.85			644	648	1.9	−5.3	−3.4
PDI **1**		−0.55	−0.78	527	536	2.3	−6.2	−3.9
PDI **2**		−0.52	−0.75	553	600	2.2	−6.1	−3.9
PDI **3**		−0.50	−0.72	562	614	2.1	−6.0	−3.9

[a]0.1 M $TBAPF_6$ in CH_2Cl_2; values vs SCE. [b]$E_g = (E_{abs} + E_{em})/2$ = optical band gap. [c]Estimated from $E_{LUMO} = 4.4$ eV $- E_{red1}$ or $E_{HOMO} = 4.4$ eV $+ E_{ox}$ and $E_{HOMO} = E_{LUMO} - E_g$

for TIPS-Pn agree with previous reports.[51] The slight differences in the reduction potentials of the acceptors are offset by the shift in E_g, giving nearly constant LUMO energies across the series. The $D_{LUMO}-A_{LUMO}$ offset was then 0.5 eV across the series, and the $D_{HOMO}-A_{HOMO}$ offset was 0.7−1.0 eV. Spectroelectrochemistry of TIPS-Pn showed that TIPS-$Pn^{+\bullet}$ has a strong absorption feature at 443 nm (Figure S2 in the Supporting Information), while the corresponding data for the $PDI^{-\bullet}$ derivatives all showed a strong characteristic absorption at 700−750 nm.[52]

The band-edge offsets between OPV electron donors and acceptors provide the free energy change essential for charge separation.[1a] Electron transfer from the photoexcitation-populated donor LUMO to the acceptor LUMO at the D−A interface is considered to be the predominant photocurrent generation pathway in BHJ OPVs having polymer donors and fullerene acceptors, wherein exciton formation is largely centered on the polymer donor, which has the greatest optical cross section.[9,53] However, in the TIPS-Pn:PDI blend films examined here, the PDI acceptors also have high extinction coefficients,[12,13] so hole transfer from the acceptor HOMO to the donor HOMO is also a possible charge separation pathway. The magnitude of this energy level LUMO−LUMO or HOMO−HOMO offset must be large enough to overcome the exciton binding energy of 0.3−0.5 eV,[53] a requirement that is clearly satisfied in the TIPS-Pn:PDI blend films (Table 1).

The TIPS-Pn:PDI **1**−**3** D−A series therefore meets the energetic requirements for efficient charge separation. However, as previous work in this field has demonstrated, achieving suitable film morphology and molecular interaction between the donor and acceptor in the photoactive layer plays a significant role in device function, even if the energetic requirements for charge separation are satisfied.[24b54]

Thin-Film Characterization. AFM scans (Figure S3a−c) show that solution-processed films of neat PDIs **2** and **3** have a root-mean-square (rms) roughness that is an order of magnitude less than those of neat PDI **1** (0.16 and 0.18 nm vs 1.3 nm, respectively). It is further evident from the AFM images of the blend films in Figure S3d−f that PDI **1**, which is the least sterically hindered PDI derivative examined here, forms the least homogeneous blend films with TIPS-Pn, while PDIs **2** and **3** form more homogeneous blend films. These differences are not as evident in the experimental film roughnesses because of the contribution of TIPS-Pn to the film morphology, which resulted in blend rms roughness values of 0.22, 0.28, and 0.19 nm for TIPS-Pn:PDI **1**, **2**, and **3** respectively. However, large, 10−20 nm wide discontinuities in the PDI **1** blend films are evident in the AFM image. These differences in film morphology suggest that PDIs **2** and **3** exhibit a decreased tendency to aggregate/precipitate from solution during film fabrication in comparison with PDI **1**.

XRD measurements showed that the neat PDI acceptors form amorphous spin-cast films while the neat TIPS-Pn films exhibit Bragg reflections, in agreement with previous studies.[45a,46b] In the as-spun blend films, which were fabricated and measured under identical conditions, the intensities of the TIPS-Pn diffraction features showed a steady decline across the series PDI **1** → **2** → **3** (Figure 3). Notably, no new features

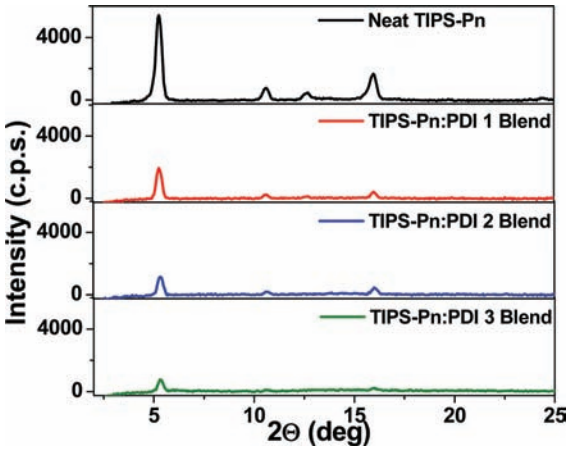

Figure 3. Θ/2Θ XRD patterns (background subtracted) for films of neat TIPS-Pn, 1:1 TIPS-Pn:PDI **1**, 1:1 TIPS-Pn:PDI **2**, and 1:1 TIPS-Pn:PDI **3**.

attributable to a discrete blend crystal structure were observed. This indicates that across the series, there are fewer TIPS-Pn domains in the blend films having long-range crystalline order. As has been discussed above, unsubstituted PDIs have large association constants for π-stacking. In the case of the TIPS-Pn:PDI **1** blend film, the strong self-association of PDI **1** results in segregated domains of polycrystalline TIPS-Pn and amorphous PDI **1**. Placing the phenyl and 3,5-di-*tert*-butylphenyl groups on the PDI at the 1- and 7-position progressively diminishes the PDI self-aggregation in proceeding from PDI **2** to PDI **3**. This makes it possible for monomeric PDIs **2** and **3** to overcome the weaker association of polycrystalline TIPS-Pn, thereby producing more homogeneous blend films. It should be noted that previous work has shown a correlation between the OPV film morphology and microstructure in polymer blends and the OPV device performance.[55]

Optical Absorption and Emission Spectra. Figure 4 compares the steady-state optical absorption and fluorescence spectra of PDIs **1**−**3** in solution and as thin films. The overall red shift of the absorption spectra of PDIs **2** and **3** in solution relative to that of PDI **1** is a well-known result of 1,7-disubstitution that twists the PDI core.[13,23] While the absorption spectrum of PDI **1** in the neat film is essentially superimposable on that of **1** in solution, the fluorescence spectrum of the PDI **1** film is broad and featureless and significantly red-shifted relative to that in solution [λ_{em}(soln) = 536 nm, λ_{em}(film) = 650 nm],

dx.doi.org/10.1021/ja2080482 | J. Am. Chem.Soc. 2012, 134, 386−397

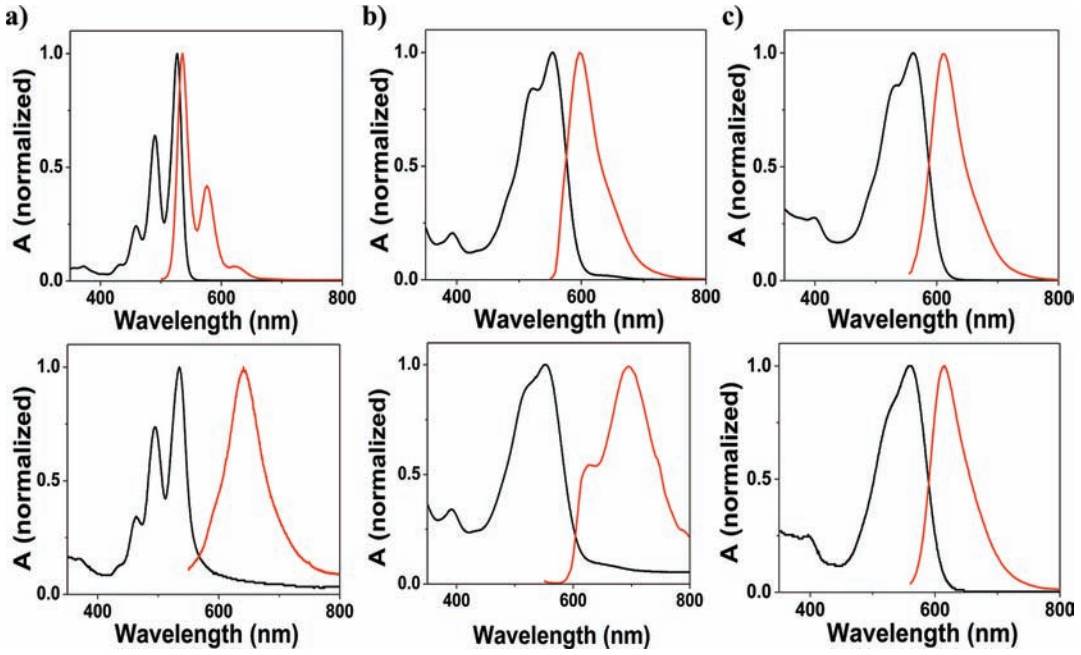

Figure 4. Optical absorption and fluorescence spectra of (top) toluene solutions and (bottom) spin-cast films of (a) neat PDI **1**, (b) neat PDI **2**, and (c) neat PDI **3**.

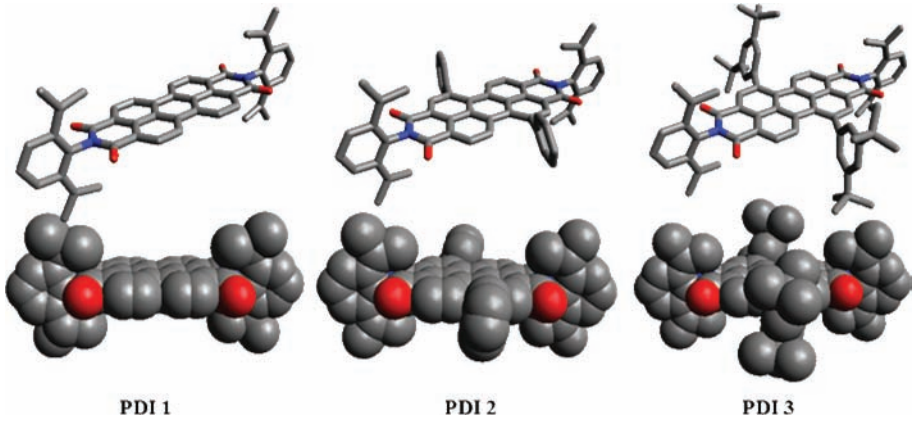

Figure 5. MM2 geometry-optimized structures of PDIs **1**–**3** illustrating the increasing steric impediment to π–π interactions between adjacent chromophores in the progression PDI **1** → **2** → **3**. H atoms have been omitted for clarity.

which is characteristic of emission from an excimer-like state.[23,56] Single-crystal XRD characterization of PDI **1** showed that the planes of the 2,6-diisopropylphenyl substituents at the imide positions are oriented nearly perpendicular to that of the perylene core,[57] which inhibits both *H*- and *J*-aggregate formation. The molecules must therefore be π-stacked with the primary transition dipoles along the N–N axes of neighboring molecules rotated significantly away from a parallel conformation, thus explaining the absence of characteristic *H*- or *J*-aggregate excitonic energy level splitting in the absorption spectrum. Since the present XRD measurements on the PDI **1** films exhibited no Bragg diffraction peaks, the π-stacked PDI **1** aggregates in the as-spun solution-processed films are either amorphous or highly disordered/nanocrystalline. In contrast, while the film and solution absorption spectra of PDI **2** are also very similar (λ_{abs} = 553 nm), their fluorescence spectra differ markedly, with the film fluorescence spectrum exhibiting a weak emission band at 614 nm assignable to the monomer and an additional excimer-like emission band at 700 nm.[23,56] Lastly, the absorption and fluorescence spectra of PDI **3** both in solution and in films are very similar [λ_{abs} = 562 nm; λ_{em}(soln) = 614 nm, λ_{em}(film) = 625 nm], suggesting that this derivative does not form strongly coupled excimer-like states in the solid film. The XRD data for the as-spun films of PDIs **2** and **3** also argue that the films are amorphous or highly disordered/nanocrystalline. Thus, the steady-state optical data suggest that as the series PDI **1** → **2** → **3** is traversed, the molecules exhibit a decreased tendency for π-stacking in the solid films, in agreement with the AFM and XRD data. The geometry-optimized structures (Figure 5) illustrate how the increasing bulk of the 1,7-substituents sterically encumbers π-stacking.

Neat TIPS-Pn films absorb strongly in the 600–700 nm region and exhibit transitions that differ significantly from those of TIPS-Pn in solution (Figure 6a), which is expected in view of the known tendency of this molecule to form two-dimensional π-stacked structures.[44] The XRD data on the neat as-spun films revealed sharp diffraction peaks, indicating that the film is polycrystalline (Figure 3). The thin-film optical spectra are

dx.doi.org/10.1021/ja2080482 | *J. Am. Chem.Soc.* 2012, 134, 386–397

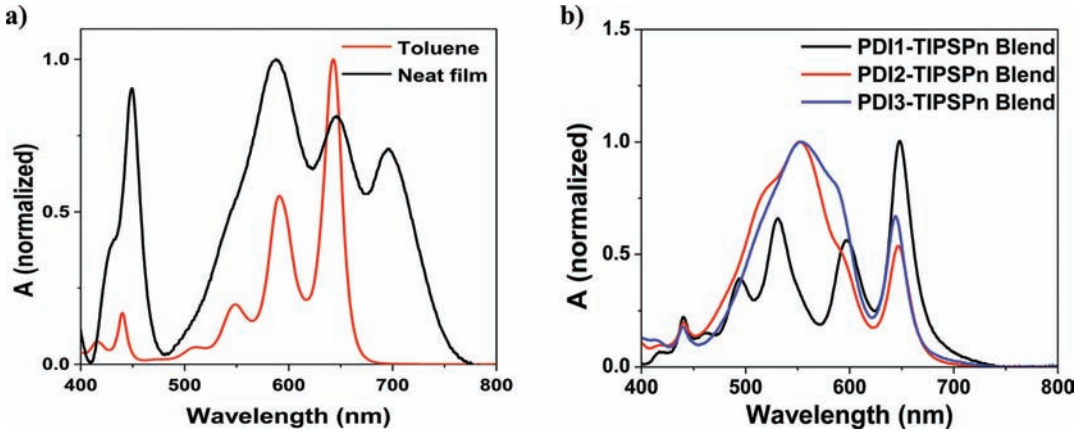

Figure 6. Steady-state optical absorption spectra of (a) TIPS-Pn in toluene solution and as a neat film and (b) 1:1 blend films of TIPS-Pn and PDI acceptors **1**–**3**.

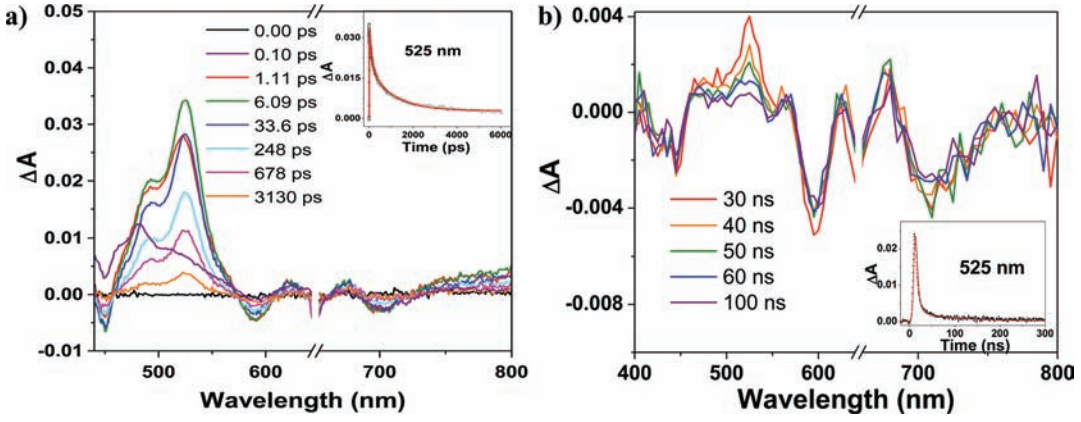

Figure 7. (a) Femtosecond and (b) nanosecond transient absorption spectra of neat TIPS-Pn films (λ_{ex} = 650 nm). The insets show the transient decay kinetics at 525 nm.

characterized by a red shift and splitting of the $S_0 \rightarrow S_1$ transition, yielding absorption maxima at 646 and 696 nm.[58] Broadening and intensity increases in the 549 and 587 nm bands were also observed, as well as an increase in intensity and a slight red shift of the 440 nm band to 449 nm. Such shifts have been observed previously in oligoacene crystals and are attributed to a mixture of Davydov splitting, vibronic coupling, and coupling between different excitonic states.[59] The ratio of the integrated intensities of the blue band (449 or 440 nm) to the red bands (500–800 nm) are similar in the film (0.15) and in solution (0.11), indicating that while some of the intensity increase in the 449 nm band may be due to small orientational preferences of the polycrystalline TIP-Pn domains in the film, for the most part the ordered polycrystalline domains have random orientations relative to one another.

The as-spun TIPS-Pn:PDI blend films absorb across the entire visible spectrum from 400 to 700 nm (Figure 6b). The absorption from 400 to 600 nm results largely from the PDI derivative, while that in the 600–700 nm range results primarily from TIPS-Pn. In contrast to neat TIPS-Pn films, the absorption spectrum of TIPS-Pn in the blend films exhibits a strong absorptive feature at 650 nm that is characteristic of amorphous TIPS-Pn[58] and strongly resembles that observed in solution (Figure 6a). The TIPS-Pn:PDI **2** blend film displays a shoulder at 600 nm relative to the PDI **2** film that is further enhanced in the TIPS-Pn:PDI **3** blend film; this shoulder may result from enhanced electronic interactions between TIPS-Pn and PDI as the films become more homogeneous. Each blend film shows essentially complete fluorescence quenching relative to the films of the neat donor and acceptors (Figure S4), which is suggestive of competitive electron transfer.

Transient Absorption Spectroscopy. The fsTA spectra of TIPS-Pn in solution (Figure S5) exhibit a broad absorption from 400 to 600 nm with a maximum at 450 nm that appears within the time scale of the instrument response and decays with τ = 17 ± 0.1 ns, in agreement with previous time-resolved fluorescence measurements.[51] This feature is attributed to the excited singlet state absorption ($S_1 \rightarrow S_n$) of ^{1}*TIPS-Pn. The same experiment was then carried out with the addition of iodomethane to enhance intersystem crossing (ISC) to the triplet state.[60] The resultant $T_1 \rightarrow T_n$ absorption spectrum of ^{3}*TIPS-Pn in solution (Figure S6) shows a strong peak at 505 nm and a secondary vibronic band at 470 nm and is in excellent agreement with the previously reported triplet excited state absorption of Pn in solution.[61] The extinction coefficient for the ^{3}*TIPS-Pn $T_1 \rightarrow T_n$ absorption, which was calculated using the ground-state bleach feature at 590 nm (ε = 10 000 M^{-1} cm^{-1} [44]) as an internal standard, was determined to be 64 000 M^{-1} cm^{-1}.

The fsTA spectra of the TIPS-Pn films (λ_{ex} = 650 nm; Figure 7a) initially display an absorption at 481 nm (100 fs), which is attributed to the $S_1 \rightarrow S_n$ transition red-shifted from its 450 nm maximum observed in solution (Figure S5a). The optical absorbances of the TIPS-Pn films were typically 0.11 at 700 nm

dx.doi.org/10.1021/ja2080482 | J. Am. Chem.Soc. 2012, 134, 386–397

with a film thickness of 8.5×10^{-6} cm. The density of crystalline TIPS-Pn obtained from its crystal structure is 1.104 g cm^{-3},[44] which gives a TIPS-Pn concentration of 1.73 M. These data yield an extinction coefficient of $\varepsilon = 7300\ M^{-1}\ cm^{-1}$ at 700 nm for TIPS-Pn in the films. Since the TIPS-Pn films have very little ground-state absorption at 481 nm (Figure 6a), the observed ΔA at 481 nm and 100 fs is due entirely to the S_1 concentration formed by the laser pulse. Thus, from the TIPS-Pn ground-state extinction coefficient, ΔA for the TIPS-Pn ground-state bleach at 700 nm, and ΔA for the $S_1 \rightarrow S_n$ transition at 481 nm and 100 fs, the calculated extinction coefficient for the TIPS-Pn $S_1 \rightarrow S_n$ transition at 481 nm is $\varepsilon = 33\,300\ M^{-1}\ cm^{-1}$.

The 481 nm absorption is rapidly replaced by a strong absorption at 525 nm that appears with a rise time (τ_R) of 1.0 ± 0.2 ps and decays with lifetimes $\tau_{D1} = 125 \pm 18$ ps (0.44), $\tau_{D2} = 1.05 \pm 0.17$ ns (0.47), and $\tau_{D3} = 80 \pm 10$ ns (0.09), as determined by fsTA and nsTA spectroscopy, respectively. The line shape of this feature is very similar to the triplet absorption in solution but is red-shifted by 20 nm. In recent years, numerous reports have proposed various spectral assignments for the triplet absorption spectrum of Pn films.[29b,d−f,62] Smith and Michl[29c] reviewed these studies in detail and found all of them to agree that the triplet absorption spectrum in a film should be red-shifted from that in solution. They further proposed that the 540 nm absorption in the Pn film transient spectrum reported by Marciniak et al.[29e] was correctly assigned to the Pn triplet state. Recently, similar red shifts were noted for the $T_1 \rightarrow T_n$ absorption spectrum of tetracene in thin solid films relative to that in solution.[63] In our experiments, therefore, the 20 nm red shift in the TIPS-Pn triplet absorption upon going from solution to a polycrystalline film is reasonable. Furthermore, previous work has shown that TIPS-Pn fluorescence is quenched in the solid film,[51] suggesting that depopulation of the photoexcited singlet state occurs by nonradiative processes.

Utilizing the observed $\Delta A = 0.0124$ and $\varepsilon = 33\,300\ M^{-1}\ cm^{-1}$ for ^{1}*TIPS-Pn at 481 nm as a measure of the initial singlet exciton concentration in the film (Figure 7a) and given that $\Delta A = 0.0342$ for ^{3}*TIPS-Pn formation at 525 nm (Figure 7a) and $\varepsilon_{max} = 64\,000\ M^{-1}\ cm^{-1}$ for ^{3}*TIPS-Pn, we calculated the triplet quantum yield as 144 ± 25%. This high ^{3}*TIPS-Pn yield along with its ultrafast formation provide strong evidence that ^{3}*TIPS-Pn forms by singlet fission. The energy level diagram in Figure 8 illustrates this process. After one TIPS-Pn is photoexcited into the S_1 state (red), it interacts with a neighboring TIPS-Pn molecule that is still in the ground state (black) to give two TIPS-Pn molecules in the T_1 state through an overall energy- and spin-conserving process.

FsTA measurements on the neat PDI films (λ_{ex} = 532 nm; Figure 9) exhibit positive absorptions at 710 nm assignable to ^{1}*PDI,[14b,d,23] which decay in concert with the recovery of the broad ground-state bleach centered at 500 nm. The 710 nm absorption is significantly broader for PDIs **2** and **3** than for PDI **1**. As noted above, this breadth is characteristic of PDI derivatives having 1,7-substituents that distort the PDI core away from planarity.[14b,d,23] These excited-state absorption changes decay rapidly to the ground state and can be fit with a biexponential function (Table 2). No longer-lived species were observed.

TIPS-Pn and PDI in the blend films were selectively photoexcited at 650 and 532 nm (Figure 10 and Figure S7, respectively) to probe any differences in the overall charge separation process. Following 650 nm excitation, the TIPS-Pn:PDI

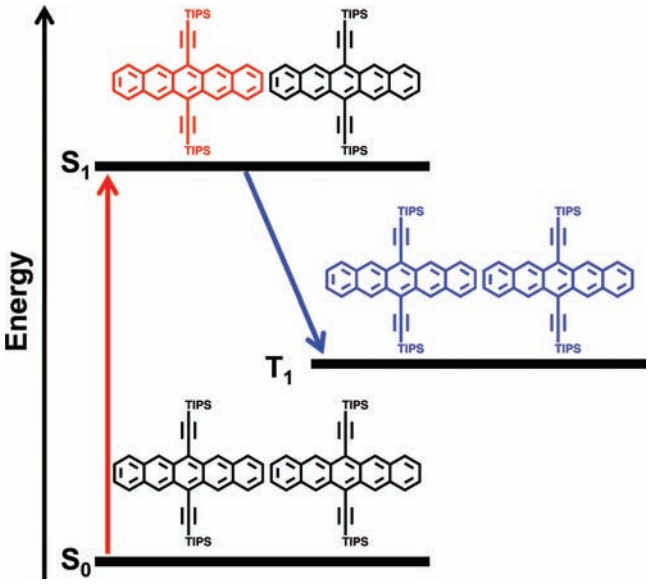

Figure 8. The SF observed in neat TIPS-Pn films occurs by excitation of one TIPS-Pn molecule to ^{1}*TIPS-Pn, which then interacts with an adjacent TIPS-Pn molecule to give two ^{3}*TIPS-Pn chromophores.

1 blend fsTA spectra (Figure 10a) display a prominent 510 nm absorption that is similar to the 525 nm absorption observed for the neat polycrystalline TIPS-Pn film. This feature forms with τ_R = 1.0 ± 0.2 ps and is most likely a result of singlet fission to produce ^{3}*TIPS-Pn. The blue shift of this transient absorption from that observed in the neat film is explained by the observation discussed above that in the blend films, the TIPS-Pn absorption resembles that of TIPS-Pn in solution because of the mixing with the PDI acceptor. Therefore, the ^{3}*TIPS-Pn absorption in the blend film accordingly lies between that in the neat film and that in solution (Figure S6). The absorption at 710 nm indicates that there is a competition between singlet fission and ultrafast electron transfer from ^{1}*TIPS-Pn to PDI. The absorption expected for TIPS-$Pn^{+\bullet}$ at 445 nm is convoluted with the first vibronic band of ^{3}*TIPS-Pn.

Following selective 650 nm TIPS-Pn excitation, fsTA spectra at 2−5.6 ns and nsTA spectra at 8−25 ns are shown for the TIPS-Pn:PDI **1** blend film in Figure S8a,b, respectively. These spectra show that the small amount of TIPS-$Pn^{+\bullet}$:$PDI^{-\bullet}$ formed is completely gone by ∼6 ns, while the concentration of the initially formed ^{3}*TIPS-Pn remains essentially unchanged over this time range. The nsTA kinetics show an instrument-limited rise time for ^{3}*TIPS-Pn, as expected on the basis of the fsTA results. Figure 10b shows that at longer times the nsTA spectra result entirely from ^{3}*TIPS-Pn, which decays biexponentially with the time constants summarized in Table 3. These results are consistent with the fact that the polycrystalline TIPS-Pn and PDI **1** domains remain largely segregated, as indicated by the XRD data and steady-state optical absorption and emission data discussed above.

In contrast to the above results, selective 650 nm photoexcitation of TIPS-Pn in the TIPS-Pn:PDI **2** and TIPS-Pn:PDI **3** blend films clearly shows the absorption bands of TIPS-$Pn^{+\bullet}$ at ∼445 nm and $PDI^{-\bullet}$ at 750 nm,[52] which appear within the 150 fs instrument response function (Figure 10c,e) and decrease on a time scale of several nanoseconds. FsTA spectra at 2−5.6 ns and nsTA spectra at 8−25 ns are shown for

dx.doi.org/10.1021/ja2080482 | J. Am. Chem.Soc. 2012, 134, 386−397

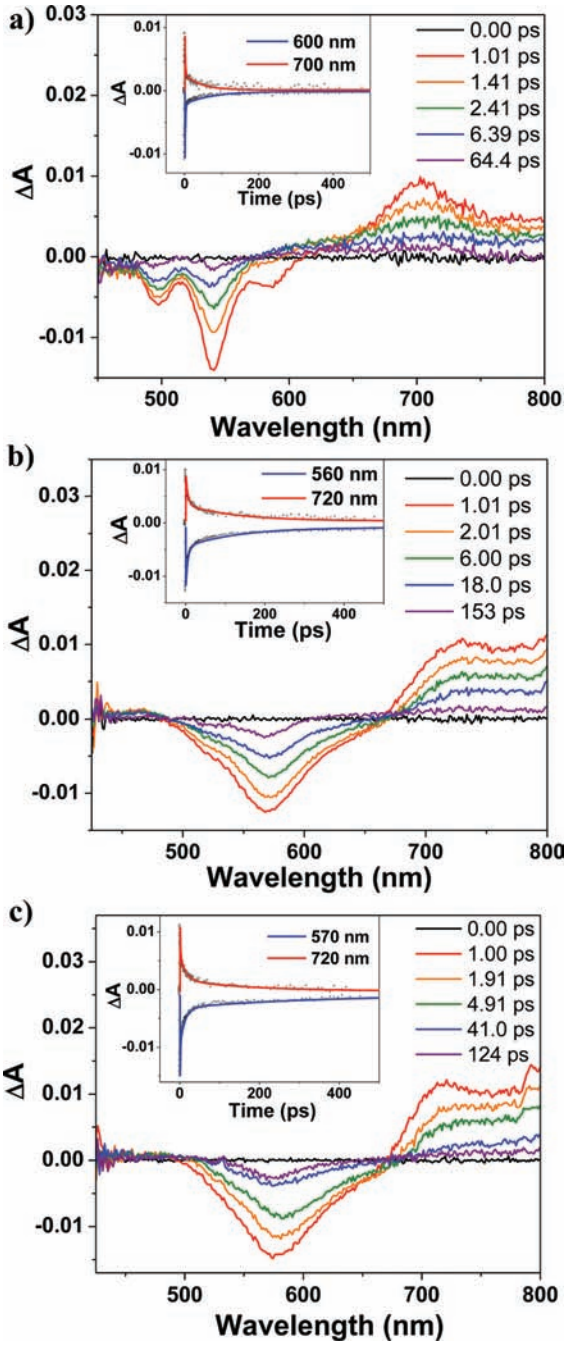

Figure 9. Femtosecond transient absorption spectra of (a) PDI **1**, (b) PDI **2**, and (c) PDI **3** films excited at 532 nm. The insets show kinetic traces and fits.

Table 2. Transient Absorption Decay Times of Neat Films of PDIs 1, 2, and 3

film	τ_{D1} (ps) (rel. amp.)	τ_{D2} (ps) (rel. amp.)
PDI **1**	1.7 ± 0.6 (74)	56 ± 12 (26)
PDI **2**	6.1 ± 1.2 (65)	133 ± 4 (35)
PDI **3**	7.8 ± 2.6 (56)	274 ± 80 (44)

TIPS-Pn:PDI **2** and TIPS-Pn:PDI **3** blend films in Figure S8c,d and Figure S8e,f, respectively. These spectra show that the $PDI^{-\bullet}$ absorption decay at 750 nm is accompanied by the formation of ^{3}*TIPS-Pn over this time range. The nsTA spectra from 19 ns to 2.5 μs are shown in Figure 10d,f. PDI and TIPS-Pn ground-state bleaching is evident in these spectra, as are $PDI^{-\bullet}$ **2** and $PDI^{-\bullet}$ **3** absorptions at 750 nm at the earliest times. The nsTA kinetics for $PDI^{-\bullet}$ decay and formation of ^{3}*TIPS-Pn in TIPS-Pn:PDI **2** and TIPS-Pn:PDI **3** blend films are shown in Figure S10c,e, respectively. The time constants for $TIPS\text{-}Pn^{+\bullet}$–$PDI^{-\bullet}$ charge recombination are τ = 6 ± 1 and 11 ± 1 ns, respectively. ^{3}*TIPS-Pn appears at 510 nm in concert with $PDI^{-\bullet}$ decay.

These same transient absorption changes appear when the PDI is excited in the blend films using 532 nm laser pulses (see Figures S7, S9, and S10b,d,f). At this excitation wavelength, we may expect to see contributions from energy transfer from ^{1}*PDI to TIPS-Pn and hole transfer from ^{1}*PDI to TIPS-Pn as well as from electron transfer from ^{1}*TIPS-Pn to PDI. It should be noted, however, that the transient absorption spectra measured using the two different excitation wavelengths are very similar, indicating that electron transfer from TIPS-Pn to ^{1}*PDI or hole transfer from ^{1}*PDI to TIPS-Pn is much faster than energy transfer from ^{1}*PDI to TIPS-Pn. The TIPS-Pn:PDI **1** blend provides one notable exception to the similar photophysics observed following 650 and 532 nm excitation, as selective 532 nm PDI photoexcitation results in charge separation with no evidence of singlet fission arising from TIPS-Pn (Figure S7a). This implies that charge separation is faster than singlet energy transfer from ^{1}*PDI to TIPS-Pn.

Ultrafast ^{3}*TIPS-Pn formation is evident in the fsTA spectra of the TIPS-Pn:PDI **1** blend films and persists in their nsTA spectra. However, the majority of ^{3}*TIPS-Pn formation in the TIPS-Pn:PDI **2** and **3** blends results from nanosecond-time-scale radical-pair ISC (RP-ISC) within the weakly spin–spin exchange-coupled $^1(TIPS\text{-}Pn^{+\bullet}\text{–}PDI^{-\bullet})$ spin-correlated radical ion pair to form $^3(TIPS\text{-}Pn^{+\bullet}\text{–}PDI^{-\bullet})$, which then undergoes charge recombination to yield either ^{3}*PDI or ^{3}*TIPS-Pn. The transient spectra in Figure 10 and Figure S7 show no evidence of the ^{3}*PDI $T_1 \rightarrow T_n$ spectrum, which has absorption features at 480 and 530 nm in solution.[65] Since the energy of ^{3}*PDI is at least 0.3 eV higher than that of ^{3}*TIPS-Pn,[29c] if any ^{3}*PDI is formed upon charge recombination, rapid energy transfer from ^{3}*PDI to TIPS-Pn most likely produces the observed ^{3}*TIPS-Pn. Geminate charge recombination to a triplet state in D–A films has been observed experimentally in polyfluorene copolymer systems[66] as well as in a variety of polymer-fullerene blends.[67] This pathway has also been studied theoretically as a general mechanism for OPV performance loss.[68]

^{3}*TIPS-Pn is derived from the population of $TIPS\text{-}Pn^{+\bullet}$–$PDI^{-\bullet}$ in which the radical ion pair distances are more than ~15 Å, an approximate distance that we have shown previously to result in a sufficiently weak spin–spin exchange interaction ($2J$) for the RP-ISC mechanism to operate.[64] Thus, the observed ^{3}*TIPS-Pn population produced by charge recombination samples the radical ion pairs that have separated to long distances at which $2J$ is small, while the closer radical ion pairs most likely recombine to the singlet ground state because they cannot undergo ISC as a result of the fact that $2J$ is large at short distances.

The decay of the 510 nm ^{3}*TIPS-Pn absorption can be fit to a sum of exponentials (Figure 11 and Table 3). The shorter-time component is attributable to triplet–triplet annihilation. It should be noted that for the TIPS-Pn:PDI **2** and TIPS-Pn:PDI **3** blends, the shorter-time component was retrieved from a weighted average of two exponential fits. Previous reports have used this method to estimate photophysical lifetimes for

dx.doi.org/10.1021/ja2080482 | J. Am. Chem.Soc. 2012, 134, 386–397

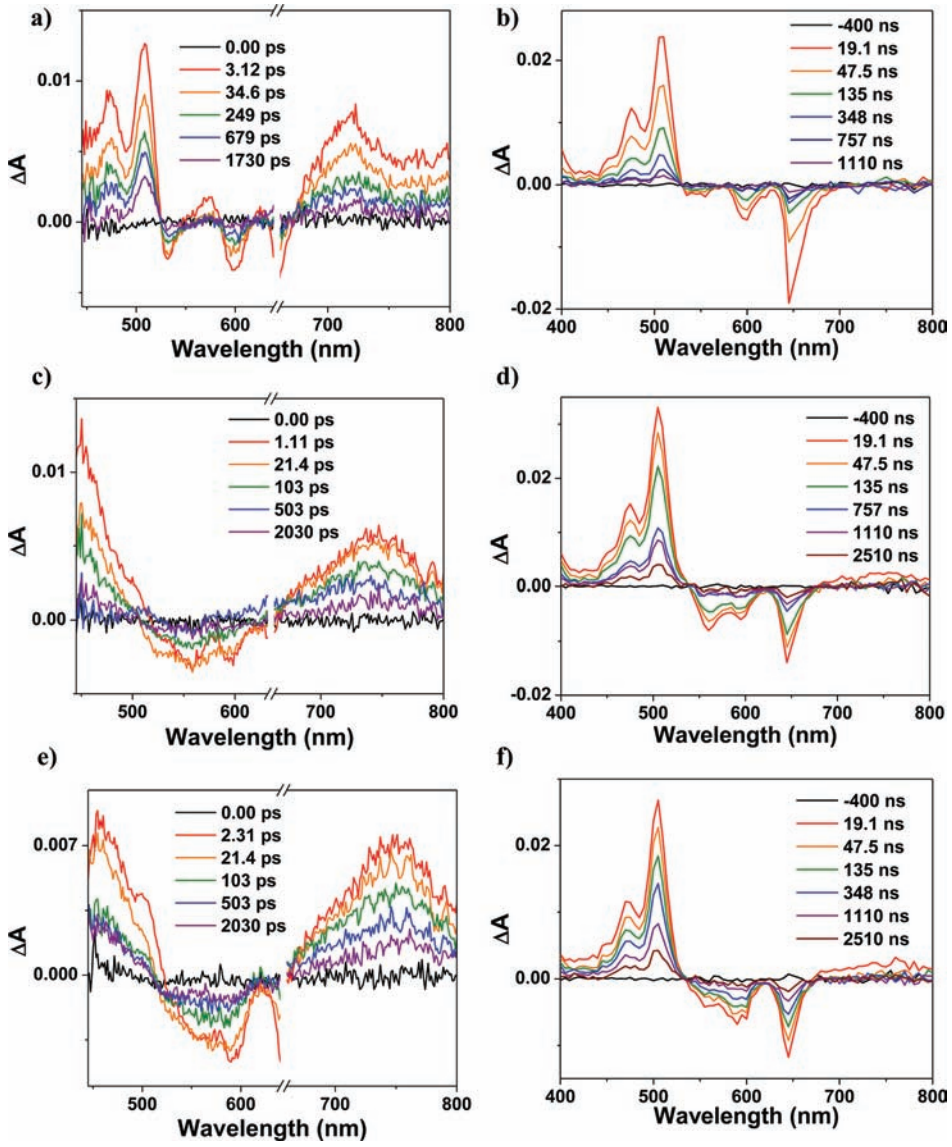

Figure 10. (a, c, e) Femtosecond and (b, d, f) nanosecond transient absorption spectra at λ_{ex} = 650 nm of 1:1 blend films of (a, b) TIPS-Pn:PDI **1**, (c, d) TIPS-Pn:PDI **2**, and (e, f) TIPS-Pn:PDI **3**.

Table 3. Summary of Exponential Kinetic Fits for the Triplet-State Feature in TIPS-Pn:PDI Blend Films (1:1 Molar Ratio) Probed at 500 nm

	τ_{D1} (ns) (rel. amp.)	τ_{D2} (ns) (rel. amp.)
TIPS-Pn:PDI **1**	55 ± 1 (0.68)	530 ± 4 (0.32)
TIPS-Pn:PDI **2**	252 ± 3 (0.66)	2480 ± 15 (0.34)
TIPS-Pn:PDI **3**	367 ± 6 (0.62)	2960 ± 30 (0.38)

annihilation processes in organic films, where nonexponential behavior is often observed.[69] The longer-time component is assigned to the decay of ^{3}*TIPS-Pn to the ground state, and the lifetimes follow the order ^{3}*TIPS-Pn:PDI **1** < ^{3}*TIPS-Pn:PDI **2** < ^{3}*TIPS-Pn:PDI **3**, a difference that can again be attributed to the diminishing degree of TIPS-Pn and PDI phase segregation as the blends become more homogeneous across the series PDI **1** → **2** → **3**.

The charge transfer dynamics of the blend films is therefore characterized (Figure 12) by competition between singlet fission within TIPS-Pn polycrystalline domains and ultrafast charge separation to form a geminate radical ion pair state

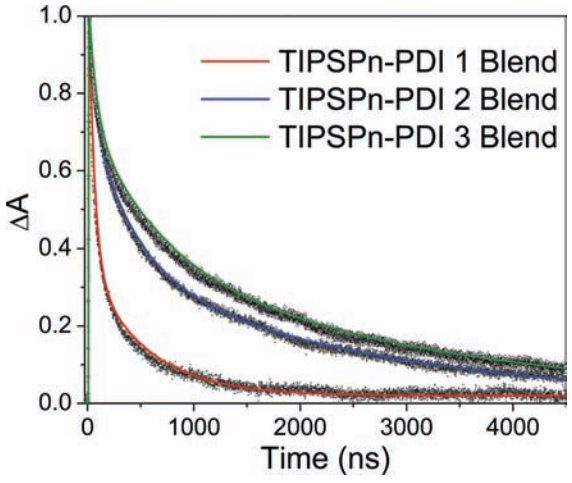

Figure 11. Nanosecond transient absorption kinetics of TIPS-Pn:PDI 1:1 blend films monitored at 510 nm.

(either by electron transfer from the ^{1}*TIPS-Pn state to the PDI or by hole transfer from the ^{1}*PDI state to TIPS-Pn)

dx.doi.org/10.1021/ja2080482 | J. Am. Chem.Soc. 2012, 134, 386–397

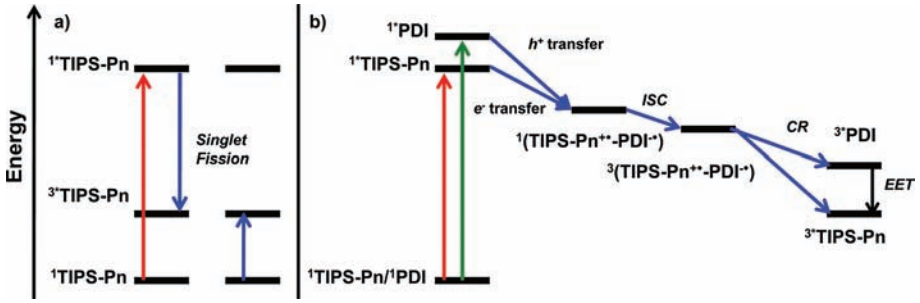

Figure 12. Multiple pathways for formation of ^{3}*TIPS-Pn: (a) Singlet fission in adjacent TIPS-Pn chromophores and (b) charge separation at the D−A interface followed by intersystem crossing (ISC) and then by charge recombination (CR) to ^{3}*TIPS-Pn either directly or via energy transfer (EET) from ^{3}*PDI.

followed by competition between recombination to ^{3}*TIPS-Pn and/or to ^{3}*PDI and formation of the singlet ground state. If ^{3}*PDI is formed, it rapidly transfers energy to the lower-lying triplet state, ^{3}*TIPS-Pn. The final ^{3}*TIPS-Pn decays at a rate that is directly correlated with the degree of TIPS-Pn crystallinity in the film, which is further dictated by the PDI acceptor aggregation.

■ CONCLUSIONS

A series of PDI acceptors with substituents providing varying degrees of steric impediment to π-stacking were synthesized by functionalizing the 1,7-positions of the perylene core with bulky aromatic groups. Optical absorption and emission spectra of the PDI films verified the expected decrease in PDI aggregation with increasing steric bulk. In addition, film characterization by AFM showed that solution processing of PDIs **2** and **3** yields smoother, more continuous films than does PDI **1**. Solution-processed blend films of PDI **1**−**3** with a TIPS-Pn donor exhibit a trend in TIPS-Pn crystallinity and molecular packing across the series that correlates closely with the trend in PDI aggregation. Upon photoexcitation, these blend films exhibit a competition between singlet fission to yield ^{3}*TIPS-Pn and ultrafast charge separation to a TIPS-Pn$^{+\bullet}$−PDI$^{-\bullet}$ geminate radical ion pair state. This state undergoes radical pair intersystem crossing followed by charge recombination, which also produces ^{3}*TIPS-Pn. These results reveal that multiple pathways produce ^{3}*TIPS-Pn, indicating that OPVs based on this system must necessarily utilize this triplet state for charge separation.

■ ASSOCIATED CONTENT

Supporting Information

Experimental and synthetic details, spectroelectrochemistry of TIPS-Pn, AFM surface characterization of PDI films, fluorescence spectra, additional TA spectra, and complete ref 35b. This material is available free of charge via the Internet at http://pubs.acs.org.

■ AUTHOR INFORMATION

Corresponding Author

m-wasielewski@northwestern.edu; t-marks@northwestern.edu

■ ACKNOWLEDGMENTS

Synthesis was supported by the Office of Naval Research under Grant N00014-05-1-0021 (M.R.W.) and BP Solar, Inc. (T.J.M., M.R.W.). Spectroscopy was supported as part of the ANSER Center, an Energy Frontier Research Center funded by the U.S. Department of Energy, Office of Science, Office of Basic Energy Sciences, under Award DE-SC0001059. Preparation of TIPS-Pn was supported by the Office of Naval Research under Grant N00014-05-1-0019. NMR and MS measurements were carried out at the Integrated Molecular Structure Education and Research Center (IMSERC) at Northwestern University. AFM measurements were carried out at the Nanoscale Integrated Fabrication, Testing and Instrumentation Center (NIFTI) at Northwestern University. XRD measurements were carried out at the J. B. Cohen X-ray Diffraction Facility supported by the MRSEC Program of the National Science Foundation (DMR-0520513) at the Materials Research Center of Northwestern University. C.R. thanks Dr. R. Ponce-Ortiz for help with XRD measurements and Drs. S. Shafaie and J. Seymour for MS measurements.

■ REFERENCES

(1) (a) Forrest, S. R. *MRS Bull.* **2005**, *30*, 28−32. (b) Tang, C. W. *Appl. Phys. Lett.* **1986**, *48*, 183−185.
(2) (a) Yang, F.; Shtein, M.; Forrest, S. R. *Nat. Mater.* **2005**, *4*, 37−41. (b) Chen, H. Y.; Hou, J. H.; Zhang, S. Q.; Liang, Y. Y.; Yang, G. W.; Yang, Y.; Yu, L. P.; Wu, Y.; Li, G. *Nat. Photonics* **2009**, *3*, 649−653.
(3) (a) Halls, J. J. M.; Walsh, C. A.; Greenham, N. C.; Marseglia, E. A.; Friend, R. H.; Moratti, S. C.; Holmes, A. B. *Nature* **1995**, *376*, 498−500. (b) Yu, G.; Gao, J.; Hummelen, J. C.; Wudl, F.; Heeger, A. J. *Science* **1995**, *270*, 1789−1791. (c) Yu, G.; Heeger, A. J. *J. Appl. Phys.* **1995**, *78*, 4510−4515.
(4) Liu, J.; Hains, A. W.; Servaites, J. D.; Ratner, M. A.; Marks, T. J. *Chem. Mater.* **2009**, *21*, 5258−5263.
(5) (a) Hains, A. W.; Ramanan, C.; Irwin, M. D.; Liu, J.; Wasielewski, M. R.; Marks, T. J. *ACS Appl. Mater. Interfaces* **2010**, *2*, 175−185. (b) Irwin, M. D.; Buchholz, B.; Hains, A. W.; Chang, R. P. H.; Marks, T. J. *Proc. Natl. Acad. Sci. U.S.A.* **2008**, *105*, 2783−2787.
(6) (a) Hains, A. W.; Liang, Z. Q.; Woodhouse, M. A.; Gregg, B. A. *Chem. Rev.* **2010**, *110*, 6689−6735. (b) Li, C.; Liu, M.; Pschirer, N. G.; Baumgarten, M.; Müllen, K. *Chem. Rev.* **2010**, *110*, 6817−6855. (c) Li, J. L.; Grimsdale, A. C. *Chem. Soc. Rev.* **2010**, *39*, 2399−2410. (d) Würthner, F.; Meerholz, K. *Chem.—Eur. J.* **2010**, *16*, 9366−9373. (e) Zhan, X.; Zhu, D. *Polym. Chem.* **2010**, *1*, 409−419. (f) Armstrong, N. R.; Veneman, P. A.; Ratcliff, E.; Placencia, D.; Brumbach, M. *Acc. Chem. Res.* **2009**, *42*, 1748−1757. (g) Kippelen, B.; Brédas, J.-L. *Energy Environ. Sci.* **2009**, *2*, 251−261.
(7) (a) Piliego, C.; Holcombe, T. W.; Douglas, J. D.; Woo, C. H.; Beaujuge, P. M.; Fréchet, J. M. J. *J. Am. Chem. Soc.* **2010**, *132*, 7595−7597. (b) Woo, C. H.; Beaujuge, P. M.; Holcombe, T. W.; Lee, O. P.; Fréchet, J. M. J. *J. Am. Chem. Soc.* **2010**, *132*, 15547−15549. (c) Liang, Y. Y.; Feng, D. Q.; Wu, Y.; Tsai, S. T.; Li, G.; Ray, C.; Yu, L. P. *J. Am. Chem. Soc.* **2009**, *131*, 7792−7799.
(8) (a) Marrocchi, A.; Silvestri, F.; Seri, M.; Facchetti, A.; Taticchia, A.; Marks, T. J. *Chem. Commun.* **2009**, 1380−1382. (b) Tamayo, A. B.; Dang, X.-D.; Walker, B.; Seo, J.; Kent, T.; Nguyen, T.-Q. *Appl. Phys.*

Lett. **2009**, *94*, No. 103301. (c) Silvestri, F.; Irwin, M. D.; Beverina, L.; Facchetti, A.; Pagani, G. A.; Marks, T. J. *J. Am. Chem. Soc.* **2008**, *130*, 4500−4502.
(9) Thompson, B. C.; Fréchet, J. M. J. *Angew. Chem., Int. Ed.* **2008**, *47*, 58−77.
(10) Wienk, M. M.; Kroon, J. M.; Verhees, W. J. H.; Knol, J.; Hummelen, J. C.; van Hal, P. A.; Janssen, R. A. J. *Angew. Chem., Int. Ed.* **2003**, *42*, 3371−3375.
(11) Reese, M. O.; Nardes, A. M.; Rupert, B. L.; Larsen, R. E.; Olson, D. C.; Lloyd, M. T.; Shaheen, S. E.; Ginley, D. S.; Rumbles, G.; Kopidakis, N. *Adv. Funct. Mater.* **2010**, *20*, 3476−3483.
(12) Langhals, H. *Helv. Chim. Acta* **2005**, *88*, 1309−1343.
(13) Würthner, F. *Chem. Commun.* **2004**, 1564−1579.
(14) (a) Bullock, J. E.; Carmieli, R.; Mickley, S. M.; Vura-Weis, J.; Wasielewski, M. R. *J. Am. Chem. Soc.* **2009**, *131*, 11919−11929. (b) Ahrens, M. J.; Sinks, L. E.; Rybtchinski, B.; Liu, W. H.; Jones, B. A.; Giaimo, J. M.; Gusev, A. V.; Goshe, A. J.; Tiede, D. M.; Wasielewski, M. R. *J. Am. Chem. Soc.* **2004**, *126*, 8284−8294. (c) Thalacker, C.; Würthner, F. *Adv. Funct. Mater.* **2002**, *12*, 209−218. (d) van der Boom, T.; Hayes, R. T.; Zhao, Y. Y.; Bushard, P. J.; Weiss, E. A.; Wasielewski, M. R. *J. Am. Chem. Soc.* **2002**, *124*, 9582−9590.
(15) (a) Zhan, X.; Facchetti, A.; Barlow, S.; Marks, T. J.; Ratner, M. A.; Wasielewski, M. R.; Marder, S. R. *Adv. Mater.* **2011**, *23*, 268−284. (b) Schmidt, R.; Oh, J. H.; Sun, Y.-S.; Deppisch, M.; Krause, A.-M.; Radacki, K.; Braunschweig, H.; Könemann, M.; Erk, P.; Bao, Z.; Würthner, F. *J. Am. Chem. Soc.* **2009**, *131*, 6215−6228. (c) Jones, B. A.; Facchetti, A.; Wasielewski, M. R.; Marks, T. J. *J. Am. Chem. Soc.* **2007**, *129*, 15259−15278. (d) Schmidt, R.; Ling, M. M.; Oh, J. H.; Winkler, M.; Könemann, M.; Bao, Z. N.; Würthner, F. *Adv. Mater.* **2007**, *19*, 3692−3695. (e) Jones, B. A.; Ahrens, M. J.; Yoon, M. H.; Facchetti, A.; Marks, T. J.; Wasielewski, M. R. *Angew. Chem., Int. Ed.* **2004**, *43*, 6363−6366.
(16) (a) Shoaee, S.; Clarke, T. M.; Huang, C.; Barlow, S.; Marder, S. R.; Heeney, M.; McCulloch, I.; Durrant, J. R. *J. Am. Chem. Soc.* **2010**, *132*, 12919−12926. (b) Shoaee, S.; An, Z. S.; Zhang, X.; Barlow, S.; Marder, S. R.; Duffy, W.; Heeney, M.; McCulloch, I.; Durrant, J. R. *Chem. Commun.* **2009**, 5445−5447. (c) Dittmer, J. J.; Marseglia, E. A.; Friend, R. H. *Adv. Mater.* **2000**, *12*, 1270−1274.
(17) (a) Howard, I. A.; Laquai, F.; Keivanidis, P. E.; Friend, R. H.; Greenham, N. C. *J. Phys. Chem. C* **2009**, *113*, 21225−21232. (b) Keivanidis, P. E.; Howard, I. A.; Friend, R. H. *Adv. Funct. Mater.* **2008**, *18*, 3189−3202.
(18) Schmidt-Mende, L.; Fechtenkötter, A.; Müllen, K.; Moons, E.; Friend, R. H.; MacKenzie, J. D. *Science* **2001**, *293*, 1119−1122.
(19) Piris, J.; de Haas, M. P.; Warman, J. M.; Müllen, K.; Fechtenkötter, A.; van de Craats, A. M.; Schmidt-Mende, L.; Friend, R. H. *Synth. Met.* **2003**, *137*, 1375−1376.
(20) (a) Anthony, J. E. *Chem. Mater.* **2011**, *23*, 583−590. (b) Rajaram, S.; Armstrong, P. B.; Kim, B. J.; Fréchet, J. M. J. *Chem. Mater.* **2009**, *21*, 1775−1777.
(21) Wasielewski, M. R. *Acc. Chem. Res.* **2009**, *42*, 1910−1921.
(22) (a) Chen, Z. J.; Debije, M. G.; Debaerdemaeker, T.; Osswald, P.; Würthner, F. *ChemPhysChem* **2004**, *5*, 137−140. (b) Liu, S. G.; Sui, G. D.; Cormier, R. A.; Leblanc, R. M.; Gregg, B. A. *J. Phys. Chem. B* **2002**, *106*, 1307−1315.
(23) Giaimo, J. M.; Lockard, J. V.; Sinks, L. E.; Scott, A. M.; Wilson, T. M.; Wasielewski, M. R. *J. Phys. Chem. A* **2008**, *112*, 2322−2330.
(24) (a) Linares, M.; Beljonne, D.; Cornil, J.; Lancaster, K.; Brédas, J.-L.; Verlaak, S.; Mityashin, A.; Heremans, P.; Fuchs, A.; Lennartz, C.; Ide, J.; Mereau, R.; Aurel, P.; Ducasse, L.; Castet, F. *J. Phys. Chem. C* **2010**, *114*, 3215−3224. (b) Zhu, X. Y.; Kahn, A. *MRS Bull.* **2010**, *35*, 443−448.
(25) Perez, M. D.; Borek, C.; Forrest, S. R.; Thompson, M. E. *J. Am. Chem. Soc.* **2009**, *131*, 9281−9286.
(26) Erwin, P.; Thompson, M. E. *Appl. Phys. Lett.* **2011**, *98*, No. 223305.
(27) Kim, I.; Haverinen, H. M.; Wang, Z. X.; Madakuni, S.; Li, J.; Jabbour, G. E. *Appl. Phys. Lett.* **2009**, *95*, No. 023305.
(28) (a) Karak, S.; Reddy, V. S.; Ray, S. K.; Dhar, A. *Org. Electron.* **2009**, *10*, 1006−1010. (b) Pandey, A. K.; Dabos-Seignon, S.; Nunzi, J. M. *Appl. Phys. Lett.* **2006**, *89*, No. 113506.
(29) (a) Wilson, M. W. B.; Rao, A.; Clark, J.; Kumar, R. S. S.; Brida, D.; Cerullo, G.; Friend, R. H. *J. Am. Chem. Soc.* **2011**, *133*, 11830−11833. (b) Rao, A.; Wilson, M. W. B.; Hodgkiss, J. M.; Albert-Seifried, S.; Bassler, H.; Friend, R. H. *J. Am. Chem. Soc.* **2010**, *132*, 12698−12703. (c) Smith, M. B.; Michl, J. *Chem. Rev.* **2010**, *110*, 6891−6936. (d) Thorsmolle, V. K.; Averitt, R. D.; Demsar, J.; Smith, D. L.; Tretiak, S.; Martin, R. L.; Chi, X.; Crone, B. K.; Ramirez, A. P.; Taylor, A. J. *Phys. Rev. Lett.* **2009**, *102*, No. 017401. (e) Marciniak, H.; Fiebig, M.; Huth, M.; Schiefer, S.; Nickel, B.; Selmaier, F.; Lochbrunner, S. *Phys. Rev. Lett.* **2007**, *99*, No. 176402. (f) Jundt, C.; Klein, G.; Sipp, B.; Lemoigne, J.; Joucla, M.; Villaeys, A. A. *Chem. Phys. Lett.* **1995**, *241*, 84−88.
(30) (a) Michl, J.; Nozik, A. J.; Chen, X.; Johnson, J. C.; Rana, G.; Akdag, A.; Schwerin, A. F. *Proc. SPIE* **2007**, *6656*, 66560E. (b) Hanna, M. C.; Nozik, A. J. *J. Appl. Phys.* **2006**, *100*, No. 074510.
(31) Singh, S.; Jones, W. J.; Siebrand, W.; Soticheff, B. P.; Schneider, W. *J. Chem. Phys.* **1965**, *42*, 330−342.
(32) (a) Swenberg, C. E.; Tracy, W. T. *Chem. Phys. Lett.* **1968**, *2*, 327−328. (b) Geacintov, N. E.; Burgos, J.; Pope, M.; Strom, C. *Chem. Phys. Lett.* **1971**, *11*, 504−508. (c) Geacintov, N. E.; Pope, M.; Vogel, F. *Phys. Rev. Lett.* **1969**, *22*, 593−596. (d) Groff, R. P.; Avakian, G. P.; Merrifield, R. E. *Phys. Rev. B* **1970**, *2*, 815−817. (e) López-Delgado, R.; Miehé, J. A.; Sipp, B. *Opt. Commun.* **1976**, *19*, 79−82. (f) Merrifield, R. E.; Aviakan, P.; Groff, R. P. *Chem. Phys. Lett.* **1969**, *3*, 155−157. (g) Pope, M.; Geacintov, N. E.; Vogel, F. *Mol. Cryst.* **1969**, *6*, 83−104. (h) Swenberg, C. E.; Van Metter, R.; Ratner, M. *Chem. Phys. Lett.* **1972**, *16*, 482−485. (i) Tomkiewicz, Y.; Groff, R. P.; Avakian, P. *J. Chem. Phys.* **1971**, *54*, 4504−4507.
(33) Von Burg, K.; Zschokke-Gränacher, I. *J. Chem. Phys.* **1979**, *70*, 3807−3811.
(34) Zenz, C.; Cerullo, G.; Lanzani, G.; Graupner, W.; Meghdadi, F.; De Silvestri, S.; Leising, G. *Synth. Met.* **1999**, *101*, 660−661.
(35) (a) Johnson, J. C.; Nozik, A. J.; Michl, J. *J. Am. Chem. Soc.* **2010**, *132*, 16302−16303. (b) Schwerin, A. F.; et al. *J. Phys. Chem. A* **2010**, *114*, 1457−1473.
(36) (a) Albrecht, W. G.; Michel-Beyerle, M. E.; Yakhot, V. *Chem. Phys.* **1978**, *35*, 193−200. (b) Albrecht, W. G.; Michel-Beyerle, M. E.; Yakhot, V. *J. Lumin.* **1979**, *20*, 147−149.
(37) Katoh, R.; Kotani, M. *Chem. Phys. Lett.* **1992**, *196*, 108−112.
(38) Najafov, H.; Lee, B.; Zhou, Q.; Feldman, L. C.; Podzorov, V. *Nat. Mater.* **2010**, *9*, 938−943.
(39) (a) Wang, C.; Tauber, M. J. *J. Am. Chem. Soc.* **2010**, *132*, 13988−13991. (b) Kingma, H.; Van Grondelle, R.; Duysens, L. N. M. *Biochim. Biophys. Acta.* **1985**, *808*, 383−399. (c) Nuijs, A. M.; Van Grondelle, R.; Joppe, H. L. P.; Van Bochove, A. C.; Duysens, L. N. M. *Biochim. Biophys. Acta* **1985**, *810*, 94−105. (d) Alster, J.; Polivka, T.; Arellano, J. B.; Chabera, P.; Vacha, F.; Psencik, J. *Chem. Phys.* **2010**, *373*, 90−97.
(40) (a) Austin, R. H.; Baker, G. L.; Etemad, S.; Thompson, R. *J. Chem. Phys.* **1989**, *90*, 6642−6646. (b) Dellepiane, G.; Comoretto, D.; Cuniberti, C. *J. Mol. Struct.* **2000**, *521*, 157−166. (c) Kraabel, B.; Hulin, D.; Aslangul, C.; Lapersonne-Meyer, C.; Schott, M. *Chem. Phys.* **1998**, *227*, 83−98. (d) Lanzani, G.; Cerullo, G.; Zavelani-Rossi, M.; De Silvestri, S.; Comoretto, D.; Musso, G.; Dellepiane, G. *Phys. Rev. Lett.* **2001**, *87*, No. 187402. (e) Wohlgenannt, M.; Graupner, W.; Osterbacka, R.; Leising, G.; Comoretto, D.; Vardeny, Z. V. *Synth. Met.* **1999**, *101*, 267−268. (f) Osterbacka, R.; Wohlgenannt, M.; Chinn, D.; Vardeny, Z. V. *Phys. Rev. B* **1999**, *60*, R11253−R11256. (g) Osterbacka, R.; Wohlgenannt, M.; Shkunov, M.; Chinn, D.; Vardeny, Z. V. *J. Chem. Phys.* **2003**, *118*, 8905−8916.
(41) (a) Zimmerman, P. M.; Zhang, Z.; Musgrave, C. B. *Nat. Chem.* **2010**, *2*, 648−652. (b) Greyson, E. C.; Stepp, B. R.; Chen, X.; Schwerin, A. F.; Paci, I.; Smith, M. B.; Akdag, A.; Johnson, J. C.; Nozik, A. J.; Michl, J.; Ratner, M. A. *J. Phys. Chem. B* **2010**, *114*, 14223−14232. (c) Paci, I.; Johnson, J. C.; Chen, X.; Rana, G.; Popovic, D.;

David, D. E.; Nozik, A. J.; Ratner, M. A.; Michl, J. *J. Am. Chem. Soc.* **2006**, *128*, 16546−16553.
(42) (a) Jadhav, P. J.; Mohanty, A.; Sussman, J.; Lee, J.; Baldo, M. A. *Nano Lett.* **2011**, *11*, 1495−1498. (b) Wu, S.-k.; Wang, P.-f. *Yingxiang Kexue Yu Guang Huaxue* **2011**, *29*, 1−10.
(43) (a) Burdett, J. J.; Müller, A. M.; Gosztola, D.; Bardeen, C. J. *J. Chem. Phys.* **2010**, *133*, 144506. (b) Müller, A. M.; Avlasevich, Y. S.; Schoeller, W. W.; Müllen, K.; Bardeen, C. J. *J. Am. Chem. Soc.* **2007**, *129*, 14240−14250. (c) Müller, A. M.; Avlasevich, Y. S.; Müllen, K.; Bardeen, C. J. *Chem. Phys. Lett.* **2006**, *421*, 518−522.
(44) Anthony, J. E.; Brooks, J. S.; Eaton, D. L.; Parkin, S. R. *J. Am. Chem. Soc.* **2001**, *123*, 9482−9483.
(45) (a) Park, S. K.; Jackson, T. N.; Anthony, J. E.; Mourey, D. A. *Appl. Phys. Lett.* **2007**, *91*, No. 063514. (b) Sheraw, C. D.; Jackson, T. N.; Eaton, D. L.; Anthony, J. E. *Adv. Mater.* **2003**, *15*, 2009−2011.
(46) (a) Palilis, L. C.; Lane, P. A.; Kushto, G. P.; Purushothaman, B.; Anthony, J. E.; Kafafi, Z. H. *Org. Electron.* **2008**, *9*, 747−752. (b) Lloyd, M. T.; Mayer, A. C.; Tayi, A. S.; Bowen, A. M.; Kasen, T. G.; Herman, D. J.; Mourey, D. A.; Anthony, J. E.; Malliaras, G. G. *Org. Electron.* **2006**, *7*, 243−248.
(47) Lloyd, M. T.; Anthony, J. E.; Malliaras, G. G. *Mater. Today* **2007**, *10*, 34−41.
(48) Connelly, N. G.; Geiger, W. E. *Chem. Rev.* **1996**, *96*, 877−910.
(49) Bullock, J. E.; Vagnini, M. T.; Ramanan, C.; Co, D. T.; Wilson, T. M.; Dicke, J. W.; Marks, T. J.; Wasielewski, M. R. *J. Phys. Chem. B* **2010**, *114*, 1794−1802.
(50) Cervini, R.; Li, X. C.; Spencer, G. W. C.; Holmes, A. B.; Moratti, S. C.; Friend, R. H. *Synth. Met.* **1997**, *84*, 359−360.
(51) Platt, A. D.; Day, J.; Subramanian, S.; Anthony, J. E.; Ostroverkhova, O. *J. Phys. Chem. C* **2009**, *113*, 14006−14014.
(52) Gosztola, D.; Niemczyk, M. P.; Svec, W.; Lukas, A. S.; Wasielewski, M. R. *J. Phys. Chem. A* **2000**, *104*, 6545−6551.
(53) Dennler, G.; Scharber, M. C.; Brabec, C. J. *Adv. Mater.* **2009**, *21*, 1323−1338.
(54) Yi, Y. P.; Coropceanu, V.; Brédas, J.-L. *J. Am. Chem. Soc.* **2009**, *131*, 15777−15783.
(55) Liu, J.; Shi, Y. J.; Yang, Y. *Adv. Funct. Mater.* **2001**, *11*, 420−424.
(56) (a) Seibt, J.; Marquetand, P.; Engel, V.; Chen, Z.; Dehrn, V.; Würthner, F. *Chem. Phys.* **2006**, *328*, 354−362. (b) Langhals, H.; Ismael, R. *Eur. J. Org. Chem.* **1998**, 1915−1917.
(57) Hadicke, E.; Graser, F. *Acta Crystallogr.* **1986**, *C42*, 195−198.
(58) Ostroverkhova, O.; Cooke, D. G.; Shcherbyna, S.; Egerton, R. F.; Hegmann, F. A.; Tykwinski, R. R.; Anthony, J. E. *Phys. Rev. B* **2005**, *71*, No. 035204.
(59) (a) Yamagata, H.; Norton, J.; Hontz, E.; Olivier, Y.; Beljonne, D.; Brédas, J.-L.; Silbey, R. J.; Spano, F. C. *J. Chem. Phys.* **2011**, *134*, 204703. (b) Spano, F. C. *Acc. Chem. Res.* **2010**, *43*, 429−439. (c) Kasha, M.; Rawls, H. R.; El-Bayoumi, M. A. *Pure Appl. Chem.* **1965**, *11*, 371−392.
(60) Turro, N. J. *Modern Molecular Photochemistry*; University Science Books: Sausalito, CA, 1991.
(61) Hellner, C.; Lindqvist, L.; Roberge, P. C. *J. Chem. Soc., Faraday Trans. 2* **1972**, *68*, 1928−1937.
(62) Kuhlman, T. S.; Kongsted, J.; Mikkelsen, K. V.; Moller, K. B.; Solling, T. I. *J. Am. Chem. Soc.* **2010**, *132*, 3431−3439.
(63) Grumstrup, E. M.; Johnson, J. C.; Damrauer, N. H. *Phys. Rev. Lett.* **2010**, *105*, No. 257403.
(64) (a) Miura, T.; Wasielewski, M. R. *J. Am. Chem. Soc.* **2011**, *133*, 2844−2847. (b) Scott, A. M.; Miura, T.; Ricks, A. B.; Dance, Z. E. X.; Giacobbe, E. M.; Colvin, M. T.; Wasielewski, M. R. *J. Am. Chem. Soc.* **2009**, *131*, 17655−17666. (c) Dance, Z. E. X.; Ahrens, M. J.; Vega, A. M.; Ricks, A. B.; McCamant, D. W.; Ratner, M. A.; Wasielewski, M. R. *J. Am. Chem. Soc.* **2008**, *130*, 830−832. (d) Weiss, E. A.; Ahrens, M. J.; Sinks, L. E.; Gusev, A. V.; Ratner, M. A.; Wasielewski, M. R. *J. Am. Chem. Soc.* **2004**, *126*, 5577−5584.
(65) (a) Giacobbe, E. M.; Mi, Q. X.; Colvin, M. T.; Cohen, B.; Ramanan, C.; Scott, A. M.; Yeganeh, S.; Marks, T. J.; Ratner, M. A.; Wasielewski, M. R. *J. Am. Chem. Soc.* **2009**, *131*, 3700−3712. (b) Ford, W. E.; Kamat, P. V. *J. Phys. Chem.* **1987**, *91*, 6373−6380.
(66) Westenhoff, S.; Howard, I. A.; Hodgkiss, J. M.; Kirov, K. R.; Bronstein, H. A.; Williams, C. K.; Greenham, N. C.; Friend, R. H. *J. Am. Chem. Soc.* **2008**, *130*, 13653−13658.
(67) Veldman, D.; Meskers, S. C. J.; Janssen, R. A. J. *Adv. Funct. Mater.* **2009**, *19*, 1939−1948.
(68) Kawatsu, T.; Coropceanu, V.; Ye, A. J.; Brédas, J.-L. *J. Phys. Chem. C* **2008**, *112*, 3429−3433.
(69) Guo, J. M.; Ohkita, H.; Benten, H.; Ito, S. *J. Am. Chem. Soc.* **2009**, *131*, 16869−16880.